Carbohydrate Polymers 103 (2014) 510–519

Contents lists available at ScienceDirect

Carbohydrate Polymers

journal homepage: www.elsevier.com/locate/carbpol

Stimulus-responsive polymeric micelles for the light-triggered release of drugs

Bin Wang, Kefu Chen, Rendang Yang, Fei Yang*, Jin Liu

State Key Lab of Pulp and Paper Engineering, South China University of Technology, Guangdong Public Laboratory of Paper Technology and Equipment, Guangzhou, China

ARTICLE INFO

Article history:
Received 4 September 2013
Received in revised form 1 December 2013
Accepted 19 December 2013
Available online 6 January 2014

Keywords:
Ethyl cellulose
Light-responsive
ATRP
Drug loading
Light-controlled release

ABSTRACT

Ethyl cellulose macroinitiator was firstly synthesized by direct acylation of ethyl cellulose with 2-bromopropionyl bromide in a room temperature. And a light-responsive triblock copolymer of ethyl cellulose-g-poly(2-hydroxyethyl methacrylate)-g-poly(spiropyran ether methacrylate) (EC-g-PHEMA-g-PSPMA) was prepared by atom transfer radial polymerization. The amphiphilic structure of the copolymer enabled it to aggregate into spherical micelles in aqueous solution with an average diameter of 100 nm. The micelles exhibited light-responsive performance because of the SPMA monomer. The hydrophobic side chain of PSPMA became hydrophilic under UV light, which decreased the average size of the micelles. Additionally, the diameters of the micelles can be recovered when subsequently irradiated with visible light. The loading and light-triggered release profiles of model drugs were also investigated, and results showed that the release behavior can be controlled by changing the light wavelength.

1. Introduction

In drug delivery, therapeutic cargos including small molecules, peptides, proteins, nucleic acids, and living cells are used to treat various sicknesses. Materials for drug delivery packages can confer specific functions, such as enhanced solubility and accurate targeting. These materials can also resolve problems of premature degradation, permeable barriers, reduced dosage, and side effects (Farokhzad & Langer, 2009; Liu, Robinson, Tabakman, Yang, & Dai, 2011; Slowing, Trewyn, Giri, & Lin, 2007; Yoo, Irvine, Discher, & Mitragotri, 2011).

New technologies and methods have recently been used to study package materials for drug delivery, including nanoparticles, nanofibers, and polymer materials (Agasti et al., 2009; Cotí et al., 2009; Ferris et al., 2009; Fu, Xu, Yao, Li, & Kang, 2009; Lee, Larson, & Lawrence, 2009; Li & Keller, 2009; Uda, Hiraishi, Ohnishi, Nakahara, & Kimura, 2010). In the successful delivery of drugs to the human body, enhancing drug encapsulation package is needed to improve biocompatibility and stability. Drug packaging using polymeric carriers solves the above problem. Polymeric designs that avoid complex circulatory pathways enable the achievement of important goals. Optimized designs can provide new insights into better therapies.

Many designed biological carrier systems (Canelas, Herlihy, & DeSimone, 2009; Kutscher et al., 2010) have been developed. Biomimetic hydrogels well control biomolecular delivery from bone defects. Specifically, designed "biomimetic" scaffolds are inspired by natural extracellular matrices, using their body as a bioreactor to regenerate bone in regulating tissue regeneration (Martino et al., 2011). Micro-needles (Kim, Park, & Prausnitz, 2012) can penetrate onto the skin and traverse skin capillaries. Consequently, drugs can be delivered to diseased areas.

In seeking effective treatment, a variety of novel drug delivery systems have been actively investigated. Among them, personalized healthcare strategies are the most promising and exciting innovations. Personalized therapy selects the right dosage for the treatment of each patient to maximize therapeutic efficacy and reduce side effects. Healthcare strategies of personalized medicine for individual patients are different. Individual patient responses therapy efficacy is not the same because of the complexity and heterogeneity of diseases and patients (Sakamoto et al., 2010). Therefore, personalized medicine designs functional carriers and collects necessary molecular data to achieve its full potential.

Several biological polymers that possess a stimulus-responsive ability are called "smart materials", which can solve personalized therapy problems. Stimulus-responsive nanocarriers deliver vehicles corresponding to external signals and "load-and-release" functions. These materials are sensitive to viruses, tumor cells, or other environmental diseases and respond to drug delivery systems. Delivery of same drug suits individual patients differently. Stimulus-responsive nanocarriers could improve drug properties

* Corresponding author. Tel.: +86 20 87110084; fax: +86 20 87111072.
E-mail address: yangfei@scut.edu.cn (F. Yang).

0144-8617/$ – see front matter © 2013 Elsevier Ltd. All rights reserved.
http://dx.doi.org/10.1016/j.carbpol.2013.12.062

by changing their response to environmental pH (Chen, Meng, Cheng, & Zhong, 2010; June, Gogoi, Eguchi, Cui, & Dowdy, 2010; Liu et al., 2011; Makhlof, Tozuka, & Takeuchi, 2009, 2011; Yuba, Harada, Sakanishi, Watarai, & Kono, 2013;Yuba et al., 2013), and temperature (Chen, Amajjahe, & Stenzel, 2009; He et al., 2011; Jiang, Li, Liu, Hennink, & Zhuo, 2012; Santos, Alves, & Mano, 2010), or through remotely applied external stimuli such as magnetic fields (Jiang et al., 2012; Lin et al., 2012; Wang et al., 2013), ultrasound (Zhang, Xia, Wang, & Li, 2009; Zhao, Du, Lu, Jin, & Ge, 2013), and light (Fan, Cheng, Ho, & Yeh, 2012; Kang et al., 2011; Knežević, Trewyn, & Lin, 2011; Lai et al., 2010). Among these stimuli, light is the most suitable for use in delivery systems because it can be manipulated with extremely high spatial and temporal precision. Additionally, the release of drugs can be rapidly accomplished at a specific time and location by specific wavelengths of light irradiation. The parameters of light intensity, wavelength, and exposure time can be established in drug delivery systems. UV light, visible light, and near infrared (NIR) can be adjusted in a treated area to induce drug release (Fomina, Sankaranarayanan, & Almutairi, 2012). Light-induced reactions do not require any chemical environmental change and can be repeated several times.

Photosensitive nanocarriers can be fabricated from a variety of biocompatible and non-toxic molecules combined with a chromophore to modulate release by switching construct properties. The therapeutic agents can be released from nanocarriers upon light exposure. Different nanocarrier including micelles, polymeric nanoparticles, hollow metal nanoparticles, and liposomes are used in respective photochemical reactions in order to facilitate release of the encapsulated bioactive agent. All light-induced reactions depending on their molecular chromophore can be divided into three: photo-isomerization, photo-cleavage, and photo-dimerization. The properties of reversible and reproducible photo-isomerization processes make chromophores attractive and be functionalized as "on–off" switch nanocarriers. Common photo-isomerization chromophore mainly include azobenzene, stilbene, and spiropyran (Tomatsu, Peng, & Kros, 2011).

Spiropyran (SP) is a structure which can control hydrophobic/hydrophilic interactions by light conversion. The hydrophobic spiropyrane state can transform into hydrophilic merocyanine state under UV light irradiation. Apart from this property, spiropyran-based materials have been widely applied in many fields, such as data storage, optical and electrical switching, and light-actuated nanovalves. SP has also been introduced into polymers to develop light-responsive micelles (Haque, Kakehi, Hara, Nagano, & Seki, 2013; Ivashenko, van Herpt, Feringa, Rudolf, & Browne, 2013; Renkecz, Mistlberger, Pawlak, Horváth, & Bakker, 2013). For example, Chen et al. reported a novel spiropyran-based block copolymer which was used to fabricate thermo- and light-responsive micelles and reverse micelles (Chen et al., 2012). Spiropyran reactions can lead to a change in the nanocarrier assembly directly or indirectly, which leads to release of drug from the nanocarrier.

A challenge in light-responsive nanocarriers is to optimize material responses and introduction into drug delivery systems to ensure that biomaterials achieved their application potential. Thus, several materials have been studied by multidisciplinary research teams in an attempt to solve such problems. These materials have been designed and engineered considering their bulk properties.

Peng et al. (Han et al., 2013) reported on amphiphilic diselenide-containing block copolymers micelles. Additionally, stable nanospheres controlled by red light can release encapsulated cargo into polymeric micelles. NIR light-responsive drug delivery platforms (Kang et al., 2011) coated with DNA cross-linked polymeric shells have been constructed. Drug delivery systems remotely controlled by NIR light can carry drugs.

In general, avoiding micellar cross-linking requires diblock copolymer micelles to be prepared in a very dilute solution. By contrast, ABC triblock polymer micelles can be achieved at higher micelle concentrations. Xu, Flores and McCormick (2011) recently synthesized the pH-responsive triblock copolymer PEO-PAPMA-PNIPAM through aqueous RAFT polymerization. Such "pH-triggered" release behavior demonstrated that triblock copolymers can be used as therapeutic nanocarriers.

In the present work, we designed and synthesized a stimulus-responsive ABC triblock polymer. First, acrylic acid-based spiropyrane monomer (SPMA) was synthesized using carboxyl-containing Sp (Sp-COOH) and hydroxyethyl methylacrylate (HEMA). The ATRP initiator was then immobilized covalently onto ethyl cellulose (EC) surface followed by 2-bromopropionyl bromide. Finally, HEMA and SPMA were grafted onto the ethyl cellulose backbone (Scheme 1). EC-g-PHEMA-g-PSPMA exhibited multiple functions resulting from its special architectures with a hydrophilic HEMA unit and a photo-responsive hydrophobic SPMA group. Considering the amphiphilic and light-responsive properties of ABC triblock polymer, they are expected to self-assemble into micelles that respond to light. The behaviors of loading and light-controlled release of drug (probe pyrene) were also investigated by irradiation at different wavelengths of light. Light-responsive triblock polymers have potential applications in controlled drug delivery.

2. Experimental

2.1. Materials

EC (M_n = 29,100 g/mol; degree of ethyl substitution = 2.1) was obtained from Aladdin and dried at 35 °C in a vacuum for 72 h before use. HEMA (Acros; 97%) was passed through a neutral aluminum oxide (250 mech) column to remove stabilizing agents.

CuBr (Acros; 97%) was purified by stirring with acetic acid and washed with methyl alcohol three times until the washings were clear. CuBr was then dried in a vacuum oven at 50 °C for 48 h. 2-Bromopropionyl bromide (BPB; 98%), Me_6tren (99%), and 2,2′-bipyridine (BPY; 98%) were purchased from Aldrich and used as received. Tetrahydrofuran (THF; Sigma, 99.9%) was dried overnight over CaH_2 and distilled under reduced pressure before use.

All other chemicals were analytical reagent grade and used without further purification. Water (18.2 MΩ) was purified with a Millipore Milli-Q system. UV and visible light irradiation were conducted at 8 W UV (354 nm) and 8 W white light (620 nm) lamps.

2.2. Synthesis of allyl-functionalized spiropyrane monomer (SPMA)

Exactly 3.84 g of SPCOOH (10 mmol), 2.68 g of HEMA (20 mmol), and 0.24 g of DMAP (2 mmol) were dissolved in 70 mL of tetrahydrofuran (THF). The solution was mixed in a three-neck flask, cooled to 0 °C in an ice–water bath, and purged with gaseous Ar. A solution containing 2.06 g (10 mmol) of dicyclohexyl carbodiimide in 30 mL of THF was added dropwise to the mixture. The following reaction was performed in the dark: the mixture was placed in an ice salt bath for 2 h and then stirred at room temperature for 24 h. Residual salt produced from the reaction was removed by filtration. The product was purified by concentration, water precipitation, benzene washing, and petroleum ether re-precipitation. The final product (3.19 g; 52% yield) was obtained using vacuum dryer.

2.3. Synthesis of an EC-Br initiator

An EC-Br macroinitiator was prepared based on the procedure shown in Scheme 1. In a typical procedure, 2.02 g (unit of

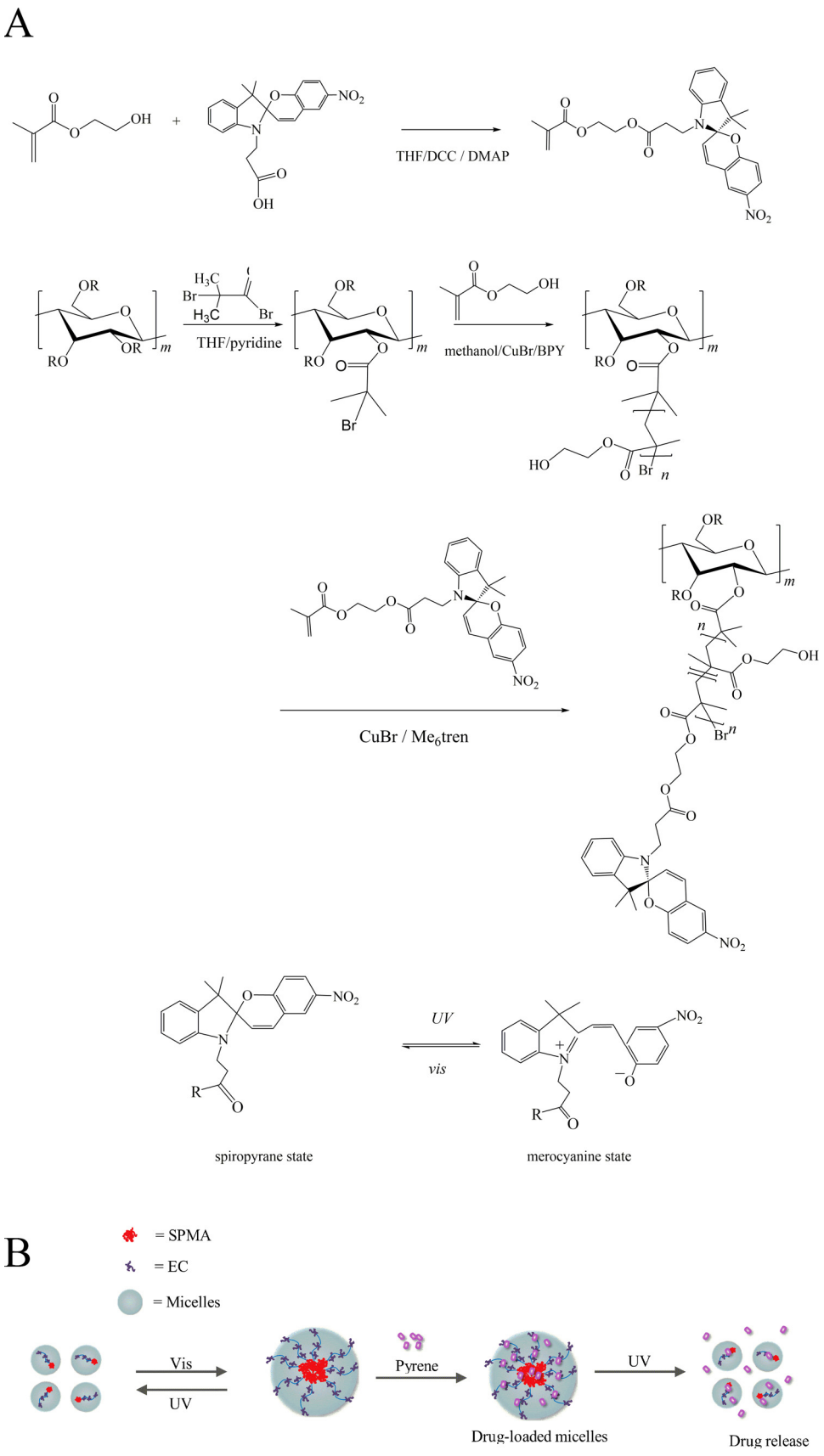

Scheme 1. (A) Synthesis of ethylcellulose graft copolymers with block. (B) Schematic illustration for the formation of micelles as well as drug loading and light controlled release of micelles.

Table 1
Preparation of EC-Br macroinitiator for ATRP.

Reactant ratio: BPB/EC[a] (mol/mol)	D_{Br} [b]	Reaction time (h)	$M_{n,NMR}$ [c] (g/mol)	$M_{n,GPC}$ [d] (g/mol)
1:2	0.08	24	30,718	29,900
1.5:1	0.11	24	31,229	35,180
2:1	0.30	24	34,954	37,000

[a] Reaction conditions: [Br]/[OH].
[b] Determined by ^{1}H NMR.
[c] Calculated by ^{1}H NMR.
[d] $M_{n,GPC}$ was monitored by GPC analysis with polystyrene standards, THF was used as mobile phase.

glucose = 10.0 mmol) of EC was dissolved in a mixture of 50 mL of dried THF and 8 mL of pyridine. Then, 2.18 g (10 mmol) of 2-bromoisobutyryl bromide in 10 mL of dried THF was slowly added dropwise into the solution at 0 °C for 1 h. The mixture was then stirred at room temperature for 24 h, and the products were precipitated with deionized water three times. The precipitate was dried in a vacuum oven at 35 °C for 72 h. The macroinitiator was characterized by IR (Nexus 470, Thermo Nicolet, USA) and ^{1}H NMR (400 MHz, AVANCE AV 400, Bruker, Switzerland) spectroscopy analyses of samples dissolved in $CDCl_3$. The experimental details and resultant EC-Br copolymers are summarized in Table 1.

2.4. Synthesis of EC-g-PHEMA by atom transfer radical polymerization (ATRP)

The synthesis of EC-g-PHEMA is shown in Scheme 1. EC-Br macroinitiator (0.52 g; 2 mmol of initiating sites) and HEMA (13.01 g; 100 mmol) were dissolved in 16.25 mL of methanol in a 100 mL flask with a magnetic stirrer. The solution was then cooled in an ice–water bath and purged with gaseous argon through three thump–thaw cycles. CuBr (0.034 g; 0.3 mmol) and 2,2-bipyridine (BPY) (0.095 g; 0.6 mmol) were added to the mixed solution under gaseous argon. The flask was then immersed in an oil bath at 30 °C for 10 h after one freeze–thump–thaw cycle with argon for ATRP reaction. After reaction completion, the mixture was exposed to air, diluted with methanol, and passed through neutral oxide alumina column to remove copper catalyst. The polymer was obtained by precipitation in deionized water and lyophilization for 24 h. The experimental details and resultant EC-g-PHEMA copolymers are summarized in Table 2.

2.5. Synthesis of EC-g-PHEMA-g-PSPMA with graft macroinitiator EC-g-PHEMA-Br using ATRP

In a typical synthesis, graft copolymer EC-g-PHEMA-Br macroinitiator (0.525 g; residual Br is 0.10 mmol) and SPMA (1.47 g, 3.0 mmol) were dissolved in 10 mL of DMF in a 25-mL flask with a magnetic stirrer. The flask was then connected with a Schlenk line where exhausting–refilling processes were performed thrice. CuBr (4.4 mg; 0.3 mmol) and Me_6tren (6.8 mg; 0.3 mmol) were then added under argon, and the reaction vessel was placed in an oil bath with a controlled temperature of 70 °C for 24 h. Polymerization was completed after cooling at room temperature. The copolymer was dialyzed against deionized water using a dialysis bag (cut off molecular weight = 14 kDa) to remove impurities. Pure graft copolymers were obtained through quick-freeze drying.

2.6. Preparation of EC-g-PHEMA-g-PSPMA micelles

Polymeric micelles were prepared by a solvent-exchange method. In a typical procedure, 25 mg of EC-g-PHEMA-g-SPMA was first dissolved in 10 mL of DMF at room temperature. Then, 5 mL deionized water was added dropwise to the solution under magnetic stirring for 3 h. The solution was then dialyzed against deionized water using a dialysis bag (cut off molecular weight = 10 kDa) for 7 days to remove DMF. Solutions were transferred into a 25 mL volumetric flask and diluted with deionized water to 1 mg/mL.

2.7. Investigation of micelles

The size of photochromic nanoparticles was measured using a Zetasizer Nano ZS instrument (Malvern Instruments, Malvern, U.K.) operating at a wavelength of 632.8 nm laser (at 90° angle) equipped with a Peltier temperature control unit. Hydrodynamic radius was calculated with the Laplace inversion program (CONTIN). All samples were filtered through membrane filter (0.45 μm) before DLS experiments.

In AFM studies, an aqueous micellar solution (1 mg/mL) was added dropwise to mica and allowed to dry at ambient temperature. Morphology pictures of micelles were recorded under ambient conditions using a multimode scanning probe microscope (Nanoscope IIIa MultiMode SPM, Japan) in tapping mode with a spring constant of 15 N/m.

2.8. Determination of critical micelle concentration (CMC)

CMC was determined using surface tension methods. Data were obtained using a contact angle meter (Dataphysics OCA40 Micro). Fresh EC-g-PHEMA-g-PSPMA micelles in deionized with concentrations of 1 mg/mL to 0.0001 mg/mL were prepared.

2.9. Irradiation experiments

Micelles were exposed to UV (354 nm) or visible (620 nm) light. Micelles (1 mg/mL) were first irradiated with 365 nm UV light for 5 min and further irradiated with visible light for 2 h. UV–visible spectrometer (Agilent 8453, USA) and DLS measurements monitored the physical and chemical changes of the micelles. UV/VIS spectroscopy confirmed the reversible progress of light-responsive micelles.

2.10. Loading of pyrene into graft copolymer micelles and its release behavior

Pyrene was selected as a hydrophobic model drug exhibiting poor water solubility, as well as a sensitive and specific spectrum. In this section, pyrene encapsulated onto micelles. UV–visible spectroscopy was used to investigate the encapsulation and release behaviors of micelles.

Pyrene-loaded micelles were prepared by a dialysis method. An intensity–concentration linear standard calibration curve was established by UV spectrophotometry. About 10 mg of polymer and 20 mg of pyrene were dissolved in 2 mL of DMSO under constant stirring. Mixed solution was dialyzed against deionized water using a dialysis bag (MWCO 3500) for 24 h with the water changed every 4 h. The amount of loaded drug in micelles (W_p) was calculated from the UV–visible absorbance of the dialysate at 303 nm wavelength.

The loading efficiency (E_L) and probe content (C_P) were defined as follows:

$$E_L = \frac{W_p}{W_t} \times 100$$

$$C_P = \frac{W_p}{W_m} \times 100$$

where W_p, W_t, and W_m are the masses of probe pyrene in micelles, total probe used, and micelles, respectively.

Table 2
Summary of the diblock copolymer obtained by changing reaction conditions.

Macroinitiator	nBr:nHEMA:nCuBr:nBPY	Time (h)	Temperature (°C)	Samples[a]	$M_{n,\,NMR}$ [b] (g/mol)
0.08	1:500:1.5:3	10	30	$EC_{0.08}$-g-$PHEMA_{32}$ *I*	34,520
0.08	1:500:1.5:3	10	40	$EC_{0.08}$-g-$PHEMA_{60}$ *II*	40,220
0.30	1:180:2:3.5	4	30	$EC_{0.30}$-g-$PHEMA_{18}$ *III*	47,230
0.46	1:80:1:3.5	–	30	Gels	–

I: $EC_{0.08}$-g-$PHEMA_{32}$ was labeled I; *II*: $EC_{0.08}$-g-$PHEMA_{60}$ was labeled II; *III*: $EC_{0.30}$-g-$PHEMA_{18}$ was labeled III.
[a] Calculated by ^{1}H NMR.
[b] Calculated by ^{1}H NMR.

After encapsulation, a dialysis bag (MWCO = 14,000) containing 5 mL of drug-loaded micelle aqueous solution was immersed in PBS solution (pH 7.4) at 37 °C in a beaker. Micelles were irradiated with different lights (354 nm UV light for 5 min or visible light for the whole time). A 2 mL PBS containing probe pyrene was sampled from the beaker at certain time intervals. UV–visible absorbance of solution was then immediately recorded. Cumulative drug release at different time intervals was determined by UV–vis spectra.

3. Results and discussion

Synthesis of EC-g-PHEMA-g-PSPMA copolymers through the ATRP reaction was shown in Scheme 1.

3.1. Preparation of SPMA

SPMA monomer was synthesized by the esterification of HEMA with carboxyl-containing spiropyran (SP-COOH) molecules. The molecular structure and synthesis route of monomer are detailed in Scheme 1. Fig. 1A shows the ^{1}H NMR spectra of SP-COOH and SPMA. Typically, chemical shift of δ = 12.3 ppm on the ^{1}H NMR spectrum (Fig. 1A (a)) of SP-COOH was carboxyl proton. Relevant signals of SP-COOH characteristic peaks at 1.0, 2.5, 3.5, and 5.9 ppm are shown in the ^{1}H NMR spectra. The ^{1}H NMR spectra of SP-COOH and SPMA showed new peak at chemical shift of δ = 1.8 ppm to 1.9 ppm and δ = 4.2 ppm, which are methyl protons in HEMA and two methylene protons in HEMA, respectively. Thus, the successful synthesis of SPMA structure by esterification was revealed.

3.2. Preparation of EC-Br macroinitiator

In a typical procedure, EC-Br macroinitiator was synthesized by EC and BPB through an acylation reaction. EC-Br macroinitiator was used for copolymerization to initiate different monomers onto EC backbone during ATRP reaction.

Degree of substitution (*DS*) of Br could be controlled by changing reactant proportion. Typically, the feeding ratio of BPB to EC was increased with increased molecular weight. Increasing molecular weight confirmed that more BPB is introduced onto EC backbone.

Fig. 1B (a and b) shows changes in FT-IR spectra of EC and EC-Br. In comparison with the native EC, EC-Br has additional band at 1751 cm^{-1}. Existence of CO band at 1751 cm^{-1} was attributed to formation of acylated ethyl cellulose. Meanwhile, the –OH groups at 3500 cm^{-1} become relatively weaker, which indicates that –OH groups on EC backbone partly reacted with 2-bromoisobutyryl bromide.

The ^{1}H NMR spectra of EC and EC-Br macroinitiator are shown in Fig. 1C (a and b). The appearance of new peak at 1.80 ppm confirmed that 2-bromopropionyl bromide was successfully grafted onto EC backbone. Relative molecular weight of EC-Br samples were obtained from their ^{1}H NMR spectra using signals at 1.8 ppm due to resonance of methyl protons in bromoisobutyryl groups and signals at 3.0 ppm to 5.0 ppm were due to resonance of H in ethyl cellulose glucose units (Fig. 1C (b)). Chemical composition of EC-Br samples, average molecular weight (M_n), and degree of substitution (*DS*) of Br group in EC unit can be calculated from the signals, which were listed in Table 1.

3.3. Preparation of EC-g-PHEMA

Graft polymerization of HEMA with EC-Br was carried with CuBr catalyst and methanol solvent to produce EC-g-PHEMA copolymers. A series of polymerizations was synthesized using macroinitiator EC-Br, catalyst CuBr, and ligand BPY (Table 2).

Comparing the FT-IR spectra of EC-Br and EC-g-PHEMA, the C=O stretching band at 1753 cm^{-1} (Fig. 1B (c)) that shifted from 1724 cm^{-1} become stronger because of the C=O groups of PHEMA side chains. The absorption peak attributed to –OH groups at around 3400 cm^{-1} became relatively wider and weaker, which indicates that HEMA was polymerized with 2-bromoisobutyryl bromide.

The ^{1}H NMR spectrum of graft copolymer is shown in Fig. 1C (c). Characteristic peaks of EC-g-PHEMA graft copolymers were readily identifiable compared with Fig. 1C (b). The signals at 1.3, 2.5, and 4.8 ppm were attributed to methyl protons of bromoisobutyryl groups and methylene protons on allyl and hydroxy protons of HEMA, respectively. ^{1}H NMR proton results indicate that PHEMA was successfully grafted on EC backbone.

In an ATRP reaction, crosslinks caused by radical–radical coupling may occur due to high concentration of chain radicals in the local area (Sui et al., 2008). Hence, to minimize coupling, macroinitiation sites should be kept at low density. Gel of polymerization mixture was easily formed and reaction was quite difficult to control during $EC_{0.46}$-g-PHEMA reaction. Experimental results obtained by various reaction conditions were listed in Table 2.

3.4. Preparation of EC-g-PHEMA-g-PSPMA

Synthesis of target EC-g-PHEMA-g-PSPMA graft polymer was readily achieved using EC-Br-g-PHEMA macroinitiator in the presence of CuBr/Me_6tren catalyst and ligand in anhydrous methyl alcohol at 70 °C. To obtain different graft lengths of PSPMA, feeding ratios were varied. Success in synthesis of EC-g-PHEMA-g-PSPMA graft copolymers was confirmed by ^{1}H NMR and FTIR spectra.

FTIR spectra of EC, EC-Br, EC-g-PHEMA, and EC-g-PHEMA-g-PSPMA are shown in Fig. 1B. Comparing with the spectrum of EC-g-PHEMA, many newly vibrating peaks were observed in the spectrum of EC-g-PHEMA-g-PSPMA (d). Peaks at 750 cm^{-1} and 808 cm^{-1} were attributed to ortho-disubstituted benzene ring and 1,2,4-substituted benzene ring in SPMA structure, respectively. Similarly, peaks at 1339 and 1516 cm^{-1} were characteristic absorptions of nitro group in spectrum of EC-g-PHEMA-g-PSPMA compared with that of EC-g-PHEMA. Hence, SPMA molecules were successfully grafted onto the EC-g-PHEMA structure.

^{1}H NMR analyses provide additional information on EC-g-PHEMA-g-PSPMA. Detail assignments of EC-g-PHEMA and EC-g-PHEMA-g-PSPMA protons are shown in Fig. 1C (c and d), respectively. Compared with EC-g-PHEMA, new signals at 7.18 and 6.71 ppm in spectrum of EC-g-PHEMA-g-PSPMA were

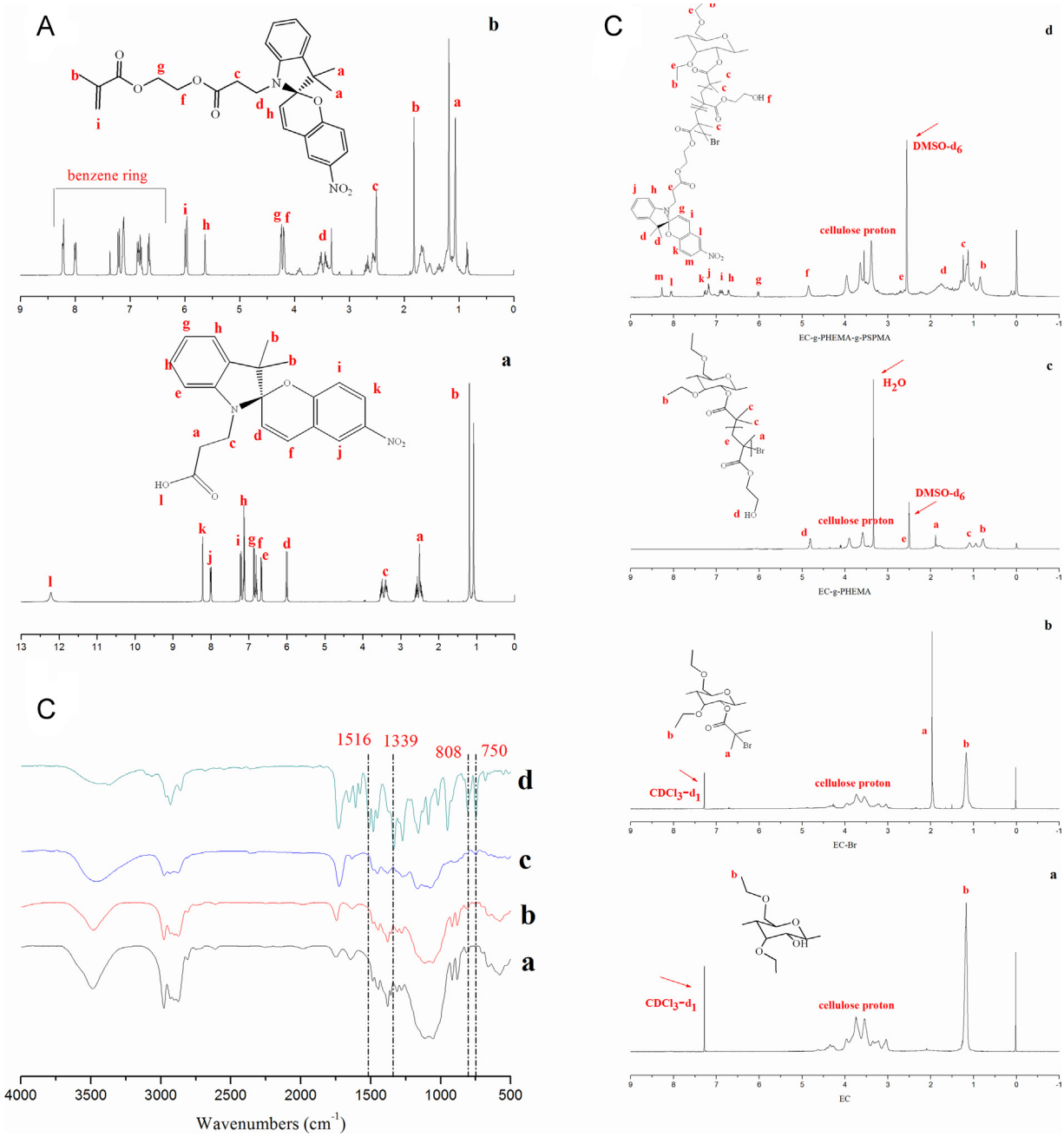

Fig. 1. (A) ^{1}H NMR spectra of SPCOOH (a), SPMA monomer (b). (B) FT-IR spectra of (a) EC, (b) EC-Br, (c) EC-g-PHEMA and (d) EC-g-PHEMA-g-PSPMA. (C) ^{1}H NMR spectra of EC (a), EC-Br (b), EC-g-PHEMA (c) and EC-g-PHEMA-PSPMA (d).

assigned to proton of ortho-disubstituted benzene ring. Similarly, characteristic signals of 1,2,4-ubstituted benzene rings in EC-g-PHEMA-g-PSPMA at 8.27, 8.05, and 7.26 ppm proved successful synthesis of EC-g-PHEMA-g-PSPMA. Graft lengths of PSPMA in the spectrum of EC-g-PHEMA-g-PSPMA can be calculated by comparing chemical shift peaks at 8.27 and 0.85 pm for H_m and H_b, respectively. From the ^{1}H NMR, block radio and average molecular weight was calculated (Table 3).

Table 3
Summary of the triblock graft polymer obtained by changing reaction conditions.

Macroinitiator[a]	nBr:nSPMA:nCuBr:nMe_6tren	Time (h)	Temperature (°C)	Samples[b]	$M_{n,\,NMR}$ [c] (g/mol)
I	0.33:10:1:1	16	70	$EC_{0.08}$-g-$PHEMA_{32}$-g-$PSPMA_{11}$	42,100
I	0.33:50:1:1	16	70	$EC_{0.08}$-g-$PHEMA_{32}$-g-$PSPMA_{15}$	44,500
II	0.33:100:1:1	12	70	$EC_{0.08}$-g-$PHEMA_{60}$-g-$PSPMA_{21}$	48,000
III	0.33:10:1:1	24	70	$EC_{0.30}$-g-$PHEMA_{18}$-g-$PSPMA_{8}$	56,140

[a] Listed in Table 2.
[b] Calculated by ^{1}H NMR.
[c] Calculated by ^{1}H NMR.

Table 4
Characteristic data of the micelles.

Sample	dn/dc[a]	$M_w \times 10^6$ [a]	N_{agg}	R_g (nm)[a]	R_h (nm)[b]	R_g/R_h
$EC_{0.08}$-g-$PHEMA_{60}$-g-$PSPMA_{21}$	0.136	5.5	116	33.4	42.3	~0.8
$EC_{0.08}$-g-$PHEMA_{32}$-g-$PSPMA_{11}$	0.136	5.7	135	36.8	54.7	~0.7
$EC_{0.08}$-g-$PHEMA_{32}$-g-$PSPMA_{15}$	0.136	6.2	139	38.6	57.0	~0.7
$EC_{0.30}$-g-$PHEMA_{18}$-g-$PSPMA_{8}$	0.136	8.5	152	45.5	57.5	~0.8

[a] Measured by GPC-MALS.
[b] Measured by DLS.

3.5. Preparation and characterization of micelle

EC-g-PHEMA-g-PSPMA copolymers comprise hydrophobic backbones (EC), hydrophobic side chains of PSPMA, and hydrophilic side chains of HEMA. Hence, EC backbones and PSPMA side chains can aggregate to form core of micelles that were stabilized with PHEMA in the shell. Micelles were prepared by dialysis method with 1.0 mg/mL concentration and then characterized by UV–vis spectrophotometer, GPC-MALS, DLS, and AFM.

Fig. 2A shows the CMC determined by relationship between surface tension and concentration. Two conclusions were obtained from Fig. 2A: First, there was a regular increase in surface tension

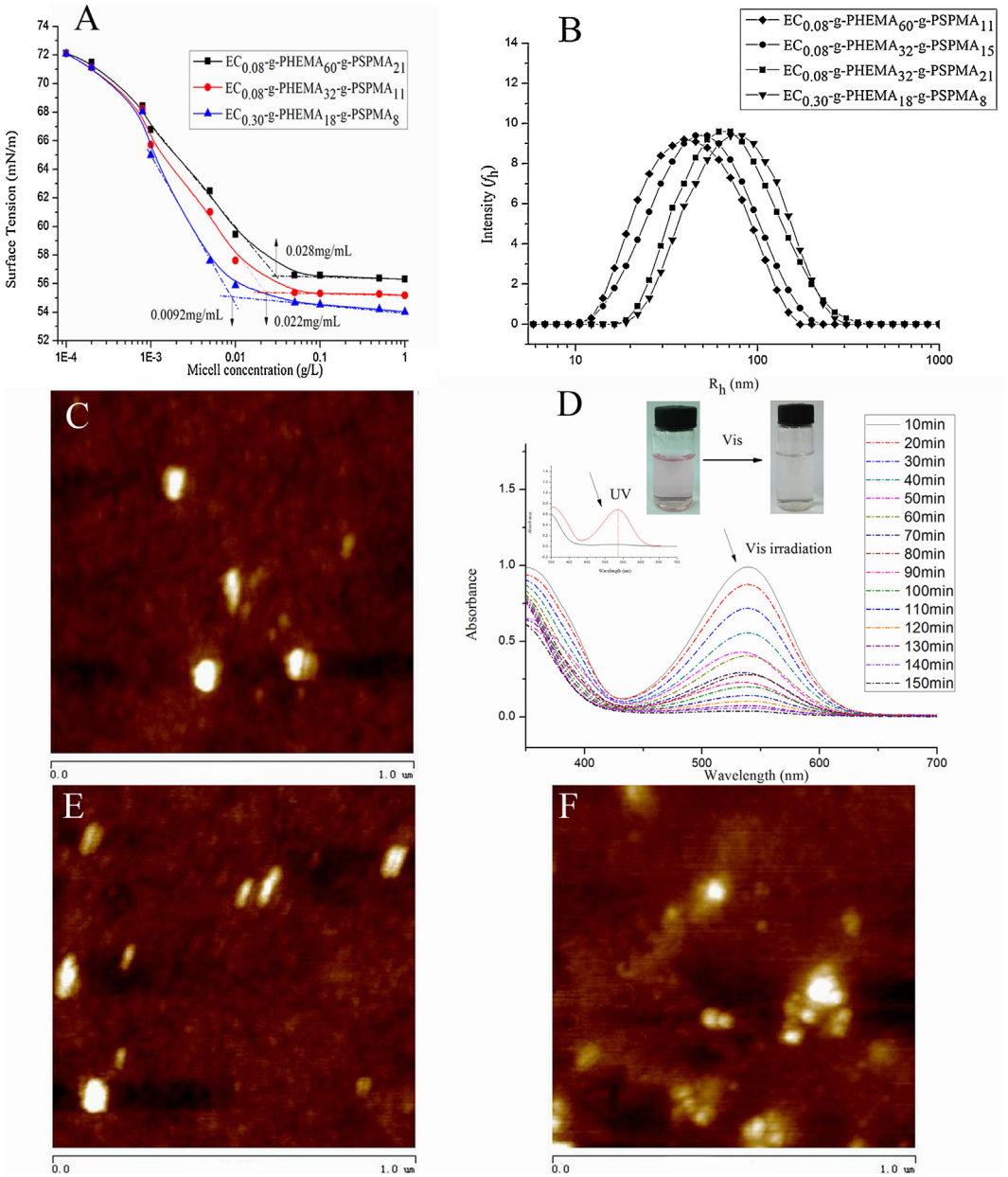

Fig. 2. (A) Surface tension of EC-g-PHEMA-g-PSPMA solution with different copolymer concentration at 25 °C. (B) Distribution of hydrodynamic radius of EC-g-PHEMA-g-PSPMA micelles. (C) AFM image of EC-g-PHEMA-g-PSPMA micelles. (D) Changes in absorption spectra for EC-g-PHEMA-g-PSPMA micelles in aqueous solution (~0.1 mg/mL) caused by vis/UV irradiation. (E) The image of micelles irradiated by visible light. (F) The image of micelles irradiated by UV light irradiation.

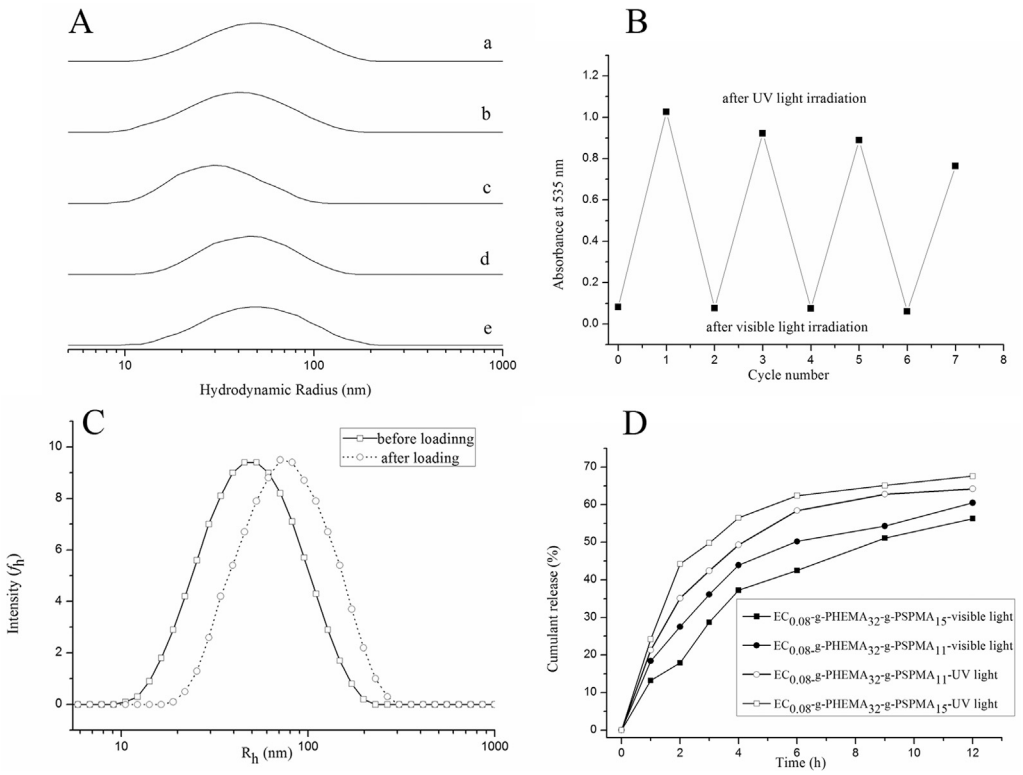

Fig. 3. (A) Hydrodynamic diameter distribution of the micelles after irradiation with different types of light: (a) initial state, (b) UV irradiation for 1 min, (c) UV irradiation for 5 min, (d) visible irradiation for 30 min, and (e) visible irradiation for 150 min. (B) The light-responsive micelles alternatively irradiated with UV light (5 min) and visible light (150 min). (C) Hydrodynamic radius distribution of the micelles ($EC_{0.08}$-g-$PHEMA_{32}$-g-$PSPMA_{11}$) before and after loading pyrene. (D) Release profile of pyrene from graft copolymer with different types of light (UV for 5 min, visible light all the time).

value with increasing number of PHEMA chains. Increasing the number of PHEMA chains in molecule strengthens hydrophilic characteristics, which decreases tendency to adsorb at air/water interface; hence, enhances surface tension. Second, CMC values of micelles depend on number of PHEMA chains grafted onto ethyl cellulose chain. CMC values were calculated by intersection point between two straight lines. Gradual increase of grafting density of PHEMA chains in EC molecules increased CMC values from 0.0092 mg/mL to 0.028 mg/mL.

DLS and AFM measurements were further performed to track macroscopic details and size of self-assemblies. Fig. 2C shows polymer self-assembled into spherical micelles in water with a diameter of about 100 nm. In addition, dynamic light scattering (DLS) measurements were performed and results are shown in Fig. 2B. Micelle diameter ranged from 84.6 nm to 115.0 nm, which agreed with data from AFM measurement. Micelle diameter depended on both the length of PHEMA side chain and graft density. For graft copolymers with similar graft density, R_h of copolymer decreased with increased PHEMA side chain. Additionally, R_h of copolymer increased with increasing graft density. R_h of $EC_{0.08}$-g-$PHEMA_{32}$-g-$PSPMA_{15}$ micelles was larger than that of $EC_{0.08}$-g-$PHEMA_{32}$-g-$PSPMA_{11}$. Given the hydrophobicity of EC backbones and PSPMA side chain, aggregates were formed and created the core of micelles. Therefore, $EC_{0.08}$-g-$PHEMA_{32}$-g-$PSPMA_{15}$ micelles contained more copolymer molecules.

GPC-MALS was conducted to ensure conclusion reliability, and results are shown in Table 4. Aggregation number (N_{agg}) can be calculated from ratio of M_w values for the micelle and unimer estimated from ^{1}H NMR measurements. Table 4 shows that N_{agg} increased by decreasing the length of PHEMA chains grafted onto the EC molecules. Less hydrophilic chain made micellar aggregation easily. R_g/R_h value reflected polymer conformation and density distribution of a particle (Niu, Liaw, Sang, & Wu, 2000). R_g/R_h value for hard uniform sphere is 0.775 (Sanwlani & Bohidar, 2013). Additionally, R_g/R_h values of micelles were 0.7 to 0.8, suggesting that micelles were close to a sphere.

3.6. Light-responsive micellization behavior of EC-g-PHEMA-g-PSPMA

Considering the introduction of light-responsive SPMA groups into polymers, self-assembly behaviors of micelles can be changed by exposing light with different wavelengths. We analyzed using UV–vis spectrophotometer, GPC-MALS, and DLS to track macroscopic details of light-responsive micellization behaviors. First, by illuminating micelles with 365 nm UV light for 5 min, as shown in Fig. 2D, micelles changed from colorless to purple. At the same time, SPMA unit in EC-g-PHEMA-g-PSPMA exhibited new absorption peak (535 nm) after UV light irradiation in UV–visible absorption spectra. A 620 nm visible light was used to irradiate micelles for 150 min. Micellar solution transformed from purple to colorless and absorption peak at 535 nm gradually disappeared.

For a complete understanding reversibility of light-induced changes in microscopic details, morphology and hydrodynamic diameters of micelles were measured by AFM and DLS while changing wavelength of light. Fig. 2E and F shows AFM images of micelles from $EC_{0.08}$-g-$PHEMA_{60}$-g-$PSPMA_{21}$ upon different irradiation of UV and visible light. Fig. 2F shows AFM image of micelles after UV irradiation for 5 min, and change in morphology is significant. Additionally, the diameter decreased to about 50 nm compared with AFM image before irradiation in Fig. 2C. After subsequent visible light irradiation for 2 h, morphology essentially returned back to that of initial micelles with about 100 nm diameter in Fig. 2E. In addition, DLS measurements analyzed the whole reversible process. Fig. 3A shows the diameter change of $EC_{0.08}$-g-$PHEMA_{60}$-g-$PSPMA_{21}$ micelles with different types of light irradiation. Diameter

Table 5
The loading efficiency and probe content of different EC-g-PHEMA-g-PSPMA micelles.

Sample	Loading efficiency (%)	Probe content (%)
$EC_{0.08}$-g-$PHEMA_{32}$-g-$PSPMA_{11}$	33.0	3.4
$EC_{0.08}$-g-$PHEMA_{32}$-g-$PSPMA_{15}$	34.9	3.5

of micelles from 84.6 nm before irradiation to 81.1 nm after exposing UV light for 1 min, and then to 73.2 nm after exposing UV light for 5 min. Influence of light on diameter is a reversible process. The diameter gradually increased to 83.3 nm and 85.2 nm after exposure to 620 nm visible light for 30 and 150 min, respectively. Reversible change in morphology of micelles can be controlled by exposing with different wavelengths of light. To test cyclic reversible response ability of micelles, sample was monitored by UV spectroscopy by alternating irradiation with UV and visible light. UV absorbance was measured at 535 nm, which demonstrated that reversible change could take place very well for several cycles in Fig. 3B.

3.7. Loading and light-responsive release of pyrene in grafted copolymer micelles

To investigate the influence of different wavelengths of light on delivery processes of micelles, probe pyrene was chosen for model drug because of its poor water solubility and spectral specificity. In the present work, $EC_{0.08}$-g-$PHEMA_{32}$-g-$PSPMA_{15}$ and $EC_{0.08}$-g-$PHEMA_{32}$-g-$PSPMA_{11}$ were chosen to investigate the process of loading and light-controlled release of drug. The loading efficiency and probe content in different EC-g-PHEMA-g-PSPMA micelles are listed in Table 5. Copolymers with higher PSPMA side chains have higher loading efficiency and probe content because of high proportion of EC and hydrophobic PSPMA side chains that had better compatibility with pyrene. Moreover, the R_h of pyrene micelles was higher than that of unloaded micelles, as shown in Fig. 3C. This finding indicated the success of pyrene loading in micelles.

The light-responsive release behavior of EC-g-PHEMA-g-PSPMA micelles was investigated under different wavelengths of light in PBS solutions at 37 °C, and results are shown in Fig. 3D. Two kinds of micelles had release behaviors within 12 h. Pyrene from $EC_{0.08}$-g-$PHEMA_{32}$-g-$PSPMA_{15}$ showed lower cumulant release than that in micelle of $EC_{0.08}$-g-$PHEMA_{32}$-g-$PSPMA_{11}$ under visible light. Consequently, hydrophobic PSPMA formed micellar aggregation, which restrains the quantity and rate of drug release. On the other hand, when the solution was irradiated with UV light for 5 min, cumulant release of pyrene in PBS solution is higher than that of under visible light. $EC_{0.08}$-g-$PHEMA_{32}$-g-$PSPMA_{15}$ showed higher cumulant release than that in $EC_{0.08}$-g-$PHEMA_{32}$-g-$PSPMA_{11}$ micelle under the same condition due to isomerization of hydrophobic PSPMA changes to hydrophilic structure under UV irradiation. Hence, aggregated micelles transformed to individual micelles resulting in higher quantity of drug release. Drug loading and light-controlled release can be accomplished in light-responsive micelles with UV or visible light (Scheme 1B).

4. Conclusion

Amphiphilic EC-g-PHEMA-g-PSPMA was prepared using ATRP approach. The graft copolymer exhibited reversible micellization induced by light change. DLS and AFM measurements revealed that the self-assembly of polymers depended on light. Additionally, polymers can self-assemble into spherical micelles with an average diameter of approximately 100 nm in aqueous solution. The micelle diameter can be controlled by UV and visible light. Micelles can be modulated by changing the ratio of hydrophilic PHEMA to hydrophobic PSPMA. Probe pyrene as a hydrophobic model drug was loaded onto micelles. Therefore, drug release could be controlled by changing light.

Acknowledgment

The authors like to acknowledge the support of the National Key Technology R&D Program (2013BAC01B03).

References

Agasti, S. S., Chompoosor, A., You, C. C., Ghosh, P., Kim, C. K., & Rotello, V. M. (2009). Photoregulated release of caged anticancer drugs from gold nanoparticles. *Journal of the American Chemical Society*, *131*(16), 5728–5729.
Canelas, D. A., Herlihy, K. P., & DeSimone, J. M. (2009). Top, down particle fabrication: Control of size and shape for diagnostic imaging and drug delivery. *Wiley Interdisciplinary Reviews: Nanomedicine and Nanobiotechnology*, *1*(4), 391–404.
Chen, C. J., Jin, Q., Liu, G. Y., Li, D. D., Wang, J. L., & Ji, J. (2012). Reversibly light-responsive micelles constructed via a simple modification of hyperbranched polymers with chromophores. *Polymer*, (53), 3695–3703.
Chen, G., Amajjahe, S., & Stenzel, M. H. (2009). Synthesis of thiol-linked neoglycopolymers and thermo-responsive glycomicelles as potential drug carrier. *Chemical Communications*, *10*, 1198–1200.
Chen, W., Meng, F., Cheng, R., & Zhong, Z. (2010). pH-sensitive degradable polymersomes for triggered release of anticancer drugs: A comparative study with micelles. *Journal of Controlled Release*, *142*(1), 40–46.
Cotí, K. K., Belowich, M. E., Liong, M., Ambrogio, M. W., Lau, Y. A., Khatib, H. A., et al. (2009). Mechanised nanoparticles for drug delivery. *Nanoscale*, *1*(1), 16–39.
Fan, N. C., Cheng, F. Y., Ho, J. A., & Yeh, C. S. (2012). Photocontrolled targeted drug delivery: Photocaged biologically active folic acid as a light, responsive tumor, targeting molecule. *Angewandte Chemie International Edition*, *51*(35), 8806–8810.
Farokhzad, O. C., & Langer, R. (2009). Impact of nanotechnology on drug delivery. *ACS Nano*, *3*(1), 16–20.
Ferris, D. P., Zhao, Y.-L., Khashab, N. M., Khatib, H. A., Stoddart, J. F., & Zink, J. I. (2009). Light-operated mechanized nanoparticles. *Journal of the American Chemical Society*, *131*(5), 1686–1688.
Fomina, N., Sankaranarayanan, J., & Almutairi, A. (2012). Photochemical mechanisms of light-triggered release from nanocarriers. *Advanced Drug Delivery Reviews*, *64*(11), 1005–1020.
Fu, G.-D., Xu, L.-Q., Yao, F., Li, G.-L., & Kang, E. T. (2009). Smart nanofibers with a photoresponsive surface for controlled release. *ACS Applied Materials & Interfaces*, *1*(11), 2424–2427.
Han, P., Li, S., Cao, W., Li, Y., Sun, Z., Wang, Z., et al. (2013). Red light responsive diselenide-containing block copolymer micelles. *Journal of Materials Chemistry B*, *1*(6), 740–743.
Haque, H. A., Kakehi, S., Hara, M., Nagano, S., & Seki, T. (2013). High density liquid crystalline azobenzene polymer brush attained by surface-initiated ring opening metathesis polymerization. *Langmuir*, *29*(25), 7571–7575.
He, X., Wu, X., Gao, C., Wang, K., Lin, S., Huang, W., et al. (2011). Synthesis and self-assembly of a hydrophilic, thermo-responsive poly(ethylene oxide) monomethyl ether-block-poly(acrylic acid)-block-poly(N-isopropylacrylamide) copolymer to form micelles for drug delivery. *Reactive and Functional Polymers*, *71*(5), 544–552.
Ivashenko, O., van Herpt, J. T., Feringa, B. L., Rudolf, P., & Browne, W. R. (2013). Electrochemical write and read functionality through oxidative dimerization of spiropyran self-assembled monolayers on gold. *The Journal of Physical Chemistry C*, *117*(36), 18567–18577.
Jiang, X., Li, L., Liu, J., Hennink, W. E., & Zhuo, R. (2012). Facile fabrication of thermo, responsive and reduction, sensitive polymeric micelles for anticancer drug delivery. *Macromolecular Bioscience*, *12*(5), 703–711.
June, R. K., Gogoi, K., Eguchi, A., Cui, X. S., & Dowdy, S. F. (2010). Synthesis of a pH-sensitive nitrilotriacetic linker to peptide transduction domains to enable intracellular delivery of histidine imidazole ring-containing macromolecules. *Journal of the American Chemical Society*, *132*(31), 10680–10682.
Kang, H., Trondoli, A. C., Zhu, G., Chen, Y., Chang, Y.-J., Liu, H., et al. (2011). Near-infrared light-responsive core–shell nanogels for targeted drug delivery. *ACS Nano*, *5*(6), 5094–5099.
Kim, Y.-C., Park, J.-H., & Prausnitz, M. R. (2012). Microneedles for drug and vaccine delivery. *Advanced Drug Delivery Reviews*, *64*(14), 1547–1568.
Knežević, N. Ž., Trewyn, B. G., & Lin, V. S. Y. (2011). Functionalized mesoporous silica nanoparticle-based visible light responsive controlled release delivery system. *Chemical Communications*, *47*(10), 2817–2819.
Kutscher, H. L., Chao, P., Deshmukh, M., Sundara Rajan, S., Singh, Y., Hu, P., et al. (2010). Enhanced passive pulmonary targeting and retention of PEGylated rigid microparticles in rats. *International Journal of Pharmaceutics*, *402*(1), 64–71.
Lai, J., Mu, X., Xu, Y., Wu, X., Wu, C., Li, C., et al. (2010). Light-responsive nanogated ensemble based on polymer grafted mesoporous silica hybrid nanoparticles. *Chemical Communications*, *46*(39), 7370–7372.
Lee, H.-M., Larson, D. R., & Lawrence, D. S. (2009). Illuminating the chemistry of life: Design, synthesis, and applications of caged and related photoresponsive compounds. *ACS Chemical Biology*, *4*(6), 409–427.

Li, M. H., & Keller, P. (2009). Stimuli-responsive polymer vesicles. *Soft Matter*, *5*(5), 927–937.
Lin, Y.-S., Huang, K. S., Yang, C. H., Wang, C. Y., Yang, Y. S., Hsu, H. C., et al. (2012). Microfluidic synthesis of microfibers for magnetic-responsive controlled drug release and cell culture. *PLOS One*, *7*(3), e33184–e33188.
Liu, R., Li, D., He, B., Xu, X., Sheng, M., Lai, Y., et al. (2011). Anti-tumor drug delivery of pH-sensitive poly(ethylene glycol)-poly(L-histidine-)-poly(L-lactide) nanoparticles. *Journal of Controlled Release*, *152*(1), 49–56.
Liu, Z., Robinson, J. T., Tabakman, S. M., Yang, K., & Dai, H. (2011). Carbon materials for drug delivery & cancer therapy. *Materials Today*, *14*(7), 316–323.
Makhlof, A., Tozuka, Y., & Takeuchi, H. (2009). pH-sensitive nanospheres for colon-specific drug delivery in experimentally induced colitis rat model. *European Journal of Pharmaceutics and Biopharmaceutics*, *72*(1), 1–8.
Makhlof, A., Tozuka, Y., & Takeuchi, H. (2011). Design and evaluation of novel pH-sensitive chitosan nanoparticles for oral insulin delivery. *European Journal of Pharmaceutical Sciences*, *42*(5), 445–451.
Martino, M. M., Tortelli, F., Mochizuki, M., Traub, S., Ben-David, D., Kuhn, G. A., et al. (2011). Engineering the growth factor microenvironment with fibronectin domains to promote wound and bone tissue healing. *Science Translatioal Medicine*, *3*(100), 100ra189.
Niu, A., Liaw, D. J., Sang, H.-C., & Wu, C. (2000). Light-scattering study of a zwitterionic polycarboxybetaine in aqueous solution. *Macromolecules*, *33*(9), 3492–3494.
Renkecz, T., Mistlberger, G., Pawlak, M., Horváth, v., & Bakker, E. (2013). Molecularly imprinted polymer microspheres containing photoswitchable spiropyran-based binding sites. *ACS Applied Materials & Interfaces*, *5*, 8537–8545.
Sakamoto, J. H., van de Ven, A. L., Godin, B., Blanco, E., Serda, R. E., Grattoni, A., et al. (2010). Enabling individualized therapy through nanotechnology. *Pharmacological Research*, *62*(2), 57–89.
Santos, J. R., Alves, N. M., & Mano, J. F. (2010). New thermo-responsive hydrogels based on poly(N-isopropylacrylamide)/hyaluronic acid semi-interpenetrated polymer networks: Swelling properties and drug release studies. *Journal of Bioactive and Compatible Polymers*, *25*(2), 169–184.
Sanwlani, S., & Bohidar, H. (2013). Differential hydration induced coil-sphere transition of gelatin chains in binary liquid solutions. *Journal of Physical Chemistry & Biophysics*, *3*(1), 100114.
Slowing, I. I., Trewyn, B. G., Giri, S., & Lin, V. Y. (2007). Mesoporous silica nanoparticles for drug delivery and biosensing applications. *Advanced Functional Materials*, *17*(8), 1225–1236.
Sui, X., Yuan, J., Zhou, M., Zhang, J., Yang, H., Yuan, W., et al. (2008). Synthesis of cellulose-graft-poly(N,N-dimethylamino-2-ethyl methacrylate) copolymers via homogeneous ATRP and their aggregates in aqueous media. *Biomacromolecules*, *9*(10), 2615–2620.
Tomatsu, I., Peng, K., & Kros, A. (2011). Photoresponsive hydrogels for biomedical applications. *Advanced Drug Delivery Reviews*, *63*(14), 1257–1266.
Uda, R. M., Hiraishi, E., Ohnishi, R., Nakahara, Y., & Kimura, K. (2010). Morphological changes in vesicles and release of an encapsulated compound triggered by a photoresponsive malachite green leuconitrile derivative. *Langmuir*, *26*(8), 5444–5450.
Wang, C. Y., Yang, C. H., Huang, K. S., Yeh, C. S., Wang, A. H. J., & Chen, C. H. (2013). Electrostatic droplets assisted in situ synthesis of superparamagnetic chitosan microparticles for magnetic-responsive controlled drug release and copper ion removal. *Journal of Materials Chemistry B: Materials for Biology and Medicine*, *1*(16), 2205–2212.
Xu, X., Flores, J. D., & McCormick, C. L. (2011). Reversible imine shell cross-linked micelles from aqueous RAFT-synthesized thermoresponsive triblock copolymers as potential nanocarriers for pH-triggered drug release. *Macromolecules*, *44*(6), 1327–1334.
Yoo, J.-W., Irvine, D. J., Discher, D. E., & Mitragotri, S. (2011). Bio-inspired, bioengineered and biomimetic drug delivery carriers. *Nature Reviews Drug Discovery*, *10*(7), 521–535.
Yuba, E., Harada, A., Sakanishi, Y., Watarai, S., & Kono, K. (2013). A liposome-based antigen delivery system using pH-sensitive fusogenic polymers for cancer immunotherapy. *Biomaterials*, *34*(12), 3042–3052.
Yuba, E., Kono, Y., Harada, A., Yokoyama, S., Arai, M., Kubo, K., et al. (2013). The application of pH-sensitive polymer-lipids to antigen delivery for cancer immunotherapy. *Biomaterials*, *34*(22), 5711–5721.
Zhang, H., Xia, H., Wang, J., & Li, Y. (2009). High intensity focused ultrasound-responsive release behavior of PLA-b-PEG copolymer micelles. *Journal of Controlled Release*, *139*(1), 31–39.
Zhao, Y.-Z., Du, L.-N., Lu, C.-T., Jin, Y.-G., & Ge, S.-P. (2013). Potential and problems in ultrasound-responsive drug delivery systems. *International Journal of Nanomedicine*, *8*, 1621–1633.